2014

High-order face-shear modes of relaxor-PbTiO3 crystals for piezoelectric motor applications

Penghong Ci
Peking University

Guoxi Liu
Peking University

Zhijiang Chen
Peking University

Shujun Zhang
Pennsylvania State University, shujun@uow.edu.au

Shuxiang Dong
Peking University

Publication Details

Ci, P., Liu, G., Chen, Z., Zhang, S. & Dong, S. (2014). High-order face-shear modes of relaxor-PbTiO3 crystals for piezoelectric motor applications. Applied Physics Letters, 104 (24), 242911-1-242911-4.

High-order face-shear modes of relaxor-PbTiO3 crystals for piezoelectric motor applications

Abstract
The face-shear vibration modes of [011] poled Zt ± 45° cut relaxor-PT crystals and their applications for linear piezoelectric motors were investigated. Unlike piezoelectric ceramics, the rotated crystal was found to exhibit asymmetric face-shear deformations, and its two high-order face-shear modes degraded into two non-isomorphic modes. As an application example, a standing wave ultrasonic linear motor ($10 \times 10 \times 2$ mm3) operating in high-order face-shear vibration modes was developed. The motor exhibits a large driving force (1.5 N) under a low driving voltage (22 Vpp). These findings could provide guidance for design of crystal resonance devices.

Disciplines
Engineering | Physical Sciences and Mathematics

Publication Details
Ci, P., Liu, G., Chen, Z., Zhang, S. & Dong, S. (2014). High-order face-shear modes of relaxor-PbTiO3 crystals for piezoelectric motor applications. Applied Physics Letters, 104 (24), 242911-1-242911-4.

High-order face-shear modes of relaxor-$PbTiO_3$ crystals for piezoelectric motor applications

Penghong Ci, Guoxi Liu, Zhijiang Chen, Shujun Zhang, and Shuxiang Dong

Citation: Appl. Phys. Lett. **104**, 242911 (2014); doi: 10.1063/1.4884652
View online: https://doi.org/10.1063/1.4884652
View Table of Contents: http://aip.scitation.org/toc/apl/104/24
Published by the American Institute of Physics

High-order face-shear modes of relaxor-$PbTiO_3$ crystals for piezoelectric motor applications

Penghong Ci,[1] Guoxi Liu,[1] Zhijiang Chen,[1] Shujun Zhang,[2,a)] and Shuxiang Dong[1,b)]
[1]*Materials Science and Engineering, College of Engineering, Peking University, Beijing 100871, China*
[2]*Materials Research Institute, The Pennsylvania State University, University Park, Pennsylvania 16802, USA*

(Received 11 April 2014; accepted 9 June 2014; published online 20 June 2014)

The face-shear vibration modes of [011] poled Zt ± 45° cut relaxor-PT crystals and their applications for linear piezoelectric motors were investigated. Unlike piezoelectric ceramics, the rotated crystal was found to exhibit asymmetric face-shear deformations, and its two high-order face-shear modes degraded into two non-isomorphic modes. As an application example, a standing wave ultrasonic linear motor ($10 \times 10 \times 2$ mm^3) operating in high-order face-shear vibration modes was developed. The motor exhibits a large driving force (1.5 N) under a low driving voltage (22 V_{pp}). These findings could provide guidance for design of crystal resonance devices. © *2014 AIP Publishing LLC*.
[http://dx.doi.org/10.1063/1.4884652]

Because of excellent piezoelectric properties, piezoelectric single crystals are currently becoming attractive in many fields, including ultrasound transducers in medical ultrasonic imaging,[1] sonar and underwater detections,[2,3] scanning tunneling microscopy, piezoelectric sensors,[4] magnetoelectric devices,[5] energy harvesters,[6,7] low-temperature actuators, and ultrasonic motors in high precision micromechanical systems.[8–11] Extensive attention has been given to relaxor-PT crystals, such as $Pb(Mg_{1/3}Nb_{2/3})O_3$-$PbTiO_3$ (PMNT), because of their superior piezoelectric characteristics over conventional $Pb(Zr,Ti)O_3$ (PZT) ceramics.[12–17] Especially, at cryogenic temperature, piezoelectric constants of piezoelectric single crystals are still superior to those of PZT ceramics at room temperature, although they also diminish as temperature decreases.[18–20]

The [011] poled Zt ± 45° cut relaxor-PT crystal exhibits large face shear piezoelectric constant d_{36} (1600 ∼ 2800 pC/N) and high electromechanical coupling factors (0.77 ∼ 0.83).[13] A resonator operating in d_{36} face shear mode also has a higher mechanical quality factor Q_m (100 ∼ 450) than that operating in d_{15} or d_{24} thickness shear mode.[13,14] In addition, the working electric field direction of a d_{36} face-shear resonator is the same as its poling direction, which can avoid the depolarization problem as occurred in d_{15} or d_{24} thickness-shear resonators.[13,14]

It is well known that a piezoelectric body in electromechanical resonance (EMR) can realize the maximum electric-to-mechanical energy conversion.[21–23] For example, an ultrasonic motor (USM) is to use EMR effect for producing precise motion. The [011] poled Zt ± 45° cut relaxor-PT crystal has potential to offer large electromechanical coupling with d_{36} face-shear vibration modes or their higher-order modes. However, because relaxor-PT crystals poled along [011] direction possess macroscopic mm2 symmetry, d_{36} face-shear vibration deformations of crystals are quite different from those of traditional piezoelectric ceramics (macroscopic 6 mm symmetry).[9,12–14,24–26] Many previous reports have pointed out excellent performances of the face shear mode and its applications, for example, face-shear-mode resonators exhibited significantly higher sensitivity to surface load changes,[24,25] and the face shear mode offered the potential to minimize the transducer device size.[9,12] In this paper, high-order d_{36} face-shear vibration modes and characteristics of [011] poled Zt ± 45° cut relaxor-PT crystals, such as deformation shapes, excitation methods, and resonance frequency features, are investigated for resonance device applications. As an application example, a standing wave USM based on high-order face-shear vibration modes is then presented.

Rhombohedral $0.72Pb(Mg_{1/3}Nb_{2/3})O_3$–$0.28PbTiO_3$ (PMNT28) single crystals were oriented along [011] and [100] directions by using a real-time back-reflection Laue system, and samples were prepared by rotating a 45° angle about Z-axis ([011] direction), and then cut into square-shape plate with dimensions of $10 \times 10 \times 2$ mm^3.[12] The obtained samples were coated with gold electrodes (Cr/Au with 100 nm thickness) on (011) faces, and poled along Z-axis under 10 kV/cm field at room temperature. In order to excite face-shear vibration modes, the top electrode of the square-plate crystal was divided into four parts (①,②,③,④), bottom electrode was a full one for electric ground, and "1–1 and 2–2" means two diagonal lines of the plate, see the schematic in the upper left inset of Fig. 1. As a comparison, piezoelectric PZT ceramic plates with the same sizes and same electrode pattern were also prepared.

First, we calculated the face-shear vibration mode and its high-order vibration modes of square-plate crystals and PZT-4 ceramics using COMSOL FEM software code (COMSOL Co., Ltd.). The material constants of crystals reported in Ref. 13 were used in our simulation. Figure 1 summarizes the simulation results, including vibrational deformation shapes of first-, second-, and third-order face-shear vibration modes (FS-1, FS-2, FS-3 modes for short) of crystals and ceramics, together with their impedance spectra and excitation methods. Unlike conventional PZT piezoelectric ceramics, rhombohedral relaxor-PT crystals possess the macroscopic mm2 symmetry when poled along [011] direction, exhibiting in-plane anisotropy.[13] It can be seen from Fig. 1

a)Email: soz1@psu.edu
b)Email: sxdong@pku.edu.cn

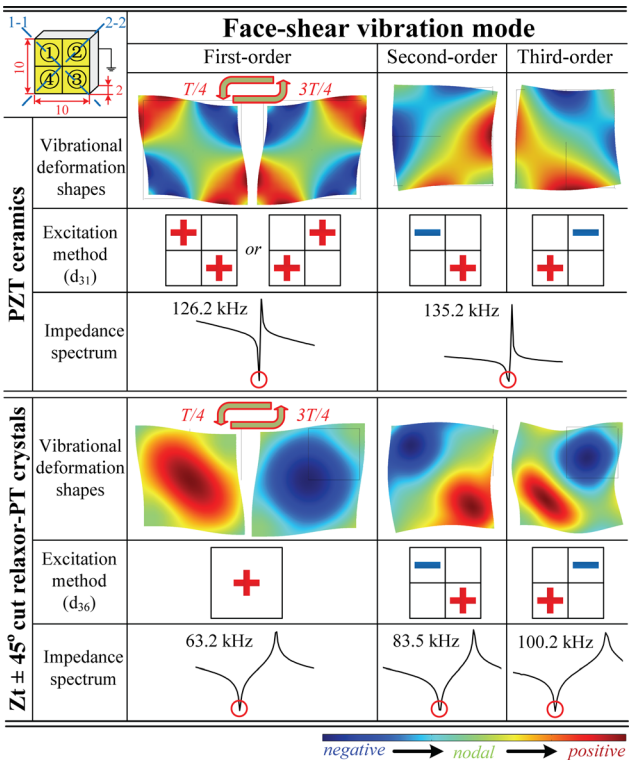

FIG. 1. Summary on the simulation results, including face-shear vibrational deformation shapes, excitation methods, and impedance spectrum of square-plate ceramics and crystals. Note that the upper left inset illustrates the schematic of the plate.

that when the FS-1 mode is excited, vibrational deformation shapes of PZT ceramics (d_{31} transverse piezoelectric effect) are symmetric in 1–1 and 2–2 directions (corresponding to T/4 and 3 T/4 cycle); while interestingly, the crystal (d_{36} face-shear piezoelectric effect) exhibits asymmetric deformation in two diagonal directions. It is found that deformation of crystals in the 1–1 direction is larger than that in the 2–2 direction. In addition, as shown in Fig. 1, when FS-2 and FS-3 modes are excited, their vibrational deformation shapes in PZT ceramics still keep in symmetry and isomorph, and their resonance frequencies (f_r) are same; while crystals exhibit asymmetric and non-isomorphic deformations for FS-2 and FS-3 modes with different resonance frequencies. That means, two isomorphic modes (FS-2 and FS-3 modes) in PZT ceramics become non-isomorphic in crystals; correspondingly, their resonance frequencies are also different. These phenomena should be attributed to the fact that PZT ceramics are isotropic polycrystal while crystals exhibit (011)-face in-plane anisotropy.[13]

Another difference in the FS-1 mode between ceramics and crystals is excitation methods, in Fig. 1. For ceramics, in order to excite the FS-1 mode, an alternating current (AC) voltage needs to be applied to electrode parts ① and ③ (or ② and ④), which will cause parts ① and ③ to shrink or elongate using d_{31} transverse piezoelectric effect. But for crystals, when an AC voltage is just applied to the whole top electrode, the FS-1 mode can be excited by using d_{36} face-shear piezoelectric effect of the crystal. However, the linear motions generated by the FS-1 mode in both ceramics and crystals at two corners are in two opposite directions in a cycle, which is not acceptable to a linear motor. Excitation methods of the FS-2 mode (or the FS-3 mode) of crystals are the same as those of ceramics, by applying one pair of AC voltages with 180° phase difference to electrode parts ① and ③ (or ② and ④), in Fig. 1. Vibrational deformation of the FS-2 mode generates a reciprocal linear motion, which can thrust a contacted slider to one direction (motion trajectories are measured in following sections). Similarly, when the FS-3 mode is excited, it produces a reverse linear motion. Thus, it is suitable for FS-2 and FS-3 modes to design linear ultrasonic actuators. In addition, on the basis of aforementioned excitation methods, we calculated impedance spectrum of these modes, in Fig. 1 (their coordinate axis were omitted). The vibration mode analysis is the basis of resonance devices, so excitation methods of these FS modes (in Fig. 1) could provide guidance for the design of face-shear resonance devices.

Next, in order to use FS-2 and FS-3 modes for generating bi-direction linear motion in a linear USM, we analyzed the dependence of resonance frequency of these modes on sizes of crystals. On the basis of the aforementioned excitation method (in Fig. 1), we measured impedance spectrum of FS-2 and FS-3 modes of crystals using an impedance analyzer (HP 4294A, Agilent Technologies, Inc., Santa Clara, CA), in Figs. 2(a) and 2(b). The measured resonance frequencies for FS-2 and FS-3 modes are 84 and 107.3 kHz, respectively. The measured values correspond well with the calculated values (83.5 and 100.2 kHz). However, we hope that the two resonance frequencies are as close as possible. The relationship between the two resonance frequencies and dimensions of crystals is, therefore, calculated using COMSOL FEM, as shown in Figs. 2(c)–2(f). Figure 2(c) illustrates the schematic of the crystal plate. It can be seen from Fig. 2(d) that as length and width of the crystal plate

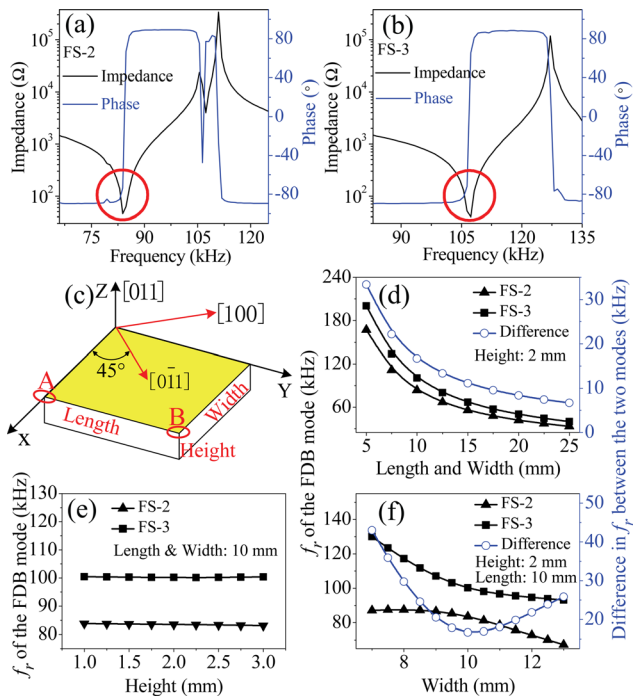

FIG. 2. Resonance frequencies of FS-2 and FS-3 modes, (a) and (b) impedance magnitude and phase spectra as a function of frequency, (c) schematic of [011] poled Zt ± 45° cut relaxor-PT crystals, (d)–(f) resonance frequencies of the two modes as a function of the dimensions of crystals.

increase, the difference in f_r between the FS-2 and FS-3 mode decreases; however, there is no across point available. In Figs. 2(e) and 2(f), it is also found that it is difficult to eliminate the difference in f_r between the FS-2 and FS-3 mode, when changing the width or height of crystals. Therefore, it seems that resonance frequency difference between the FS-2 and FS-3 mode is unavoidable in the crystal plate.

Then, to further determine motion trajectories of the two non-isomorphic in-plane face-shear vibration modes, we measured the displacement amplitudes and phases of crystals using laser Doppler Vibrometer (Polytec, PSV-400 Scanning Vibrometer), based on the aforementioned driving method and the obtained f_r, as illustrated in Fig. 1. Figures 3(a) and 3(c) illustrate a series of measured displacement amplitudes (colored contours) of FS-2 and FS-3 modes corresponding to T/4 and 3 T/4 cycle, in which the color indicates the degree of deformation. And the deformation shapes (red contours) were also calculated by COMSOL FEM. Experimental displacement amplitudes correspond well with the calculated deformation shapes. According to measured displacement amplitudes of the FS-2 mode at different moments (phases) in a cycle (in Fig. 3(a)), displacement amplitudes of crystals at the Corners (A) and (B) in the vertical and horizontal directions can be obtained at different phases, thus their resultant motion trajectories are shown in Fig. 3(b). Note that Fig. 2(c) illustrates positions of the Corners (A) and (B). Similarly, motion trajectories in the FS-3 mode at the Corners (A) and (B) can also be obtained, as shown in Fig. 3(d). It is clearly found that the two resultant motion trajectories for FS-2 and FS-3 modes are reciprocal, linear, and also orthogonal, which can be used for thrusting a contacted slider toward to the left or right direction. Note the resultant motion trajectory of the Corner (B) is orthogonal with that of the Corner (A) in the FS-2 mode, which may cause a drag effect to linear motion. Fortunately, displacement amplitude

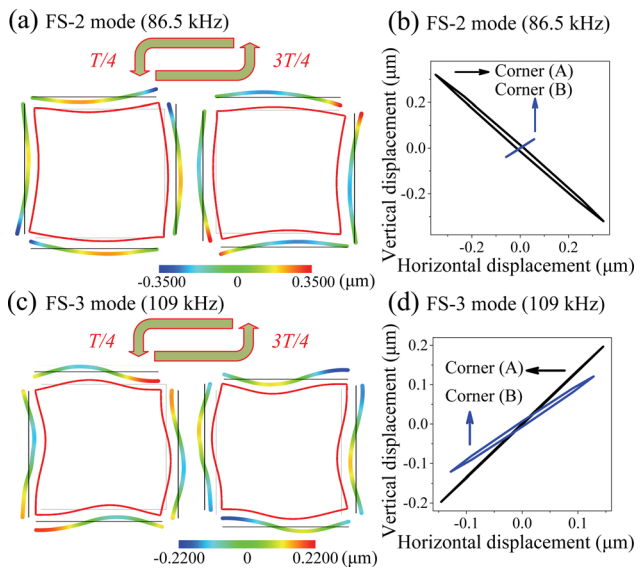

FIG. 3. Vibration amplitude properties of FS-2 and FS-3 modes, (a) and (c) measured displacement amplitudes (colored contours) and simulated deformation shapes (red contours), corresponding to T/4 and 3 T/4 cycle, (b) and (d) measured motion trajectories of the Corners (A) and (B) (see the schematic in Fig. 2(c)).

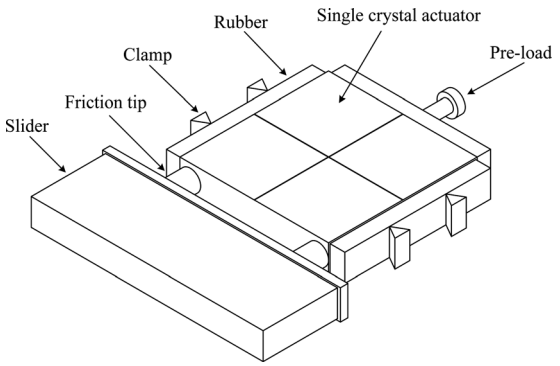

FIG. 4. Configuration of the standing wave linear USM.

of the Corner (B) excited in the FS-2 mode is much smaller than that of the Corner (A). Therefore, this unfavorable factor is ignored for a linear USM.

Finally, after assembling the rotated-crystal resonance actuator operating in two orthogonal vibration modes (FS-2 and FS-3) into a USM setup, we obtained a standing wave linear USM prototype, as shown in Fig. 4. Excitation methods of FS-2 and FS-3 modes in the crystal square-plate are illustrated in Fig. 1. We measured the maximum mechanical load and no-load motion speed of the USM in two directions as a function of working frequency under an applied voltage of 22 V_{pp}, in Figs. 5(a) and 5(c). Figures 5(b) and 5(d) present the motion speed and efficiency of the USM in two directions as a function of mechanical load. It is found that the maximum driving force, the maximum non-load motion speed, and the maximum efficiency of the USM under a low applied AC voltage of 22 V_{pp} (i.e., an applied electric field of 11 V_{pp}/mm) are 1.5 N, 100 mm/s, and 7%, respectively. One feature of the USM is its relatively low driving voltage, but large generating force, which is apparently superior to a face-shear mode motor.[14] This reported motor presented only 1.0 N driving force under an applied voltage of 50 V_{pp}.[14] Even comparing with a square-plate piezo-ceramic motor with a larger size of $15 \times 15 \times 2$ mm^3, our USM also shows a larger unit volume driving force under a lower driving voltage.[22,23,27] In addition, due to its non-coupled working modes, it is reasonable to infer that the USM is not affected

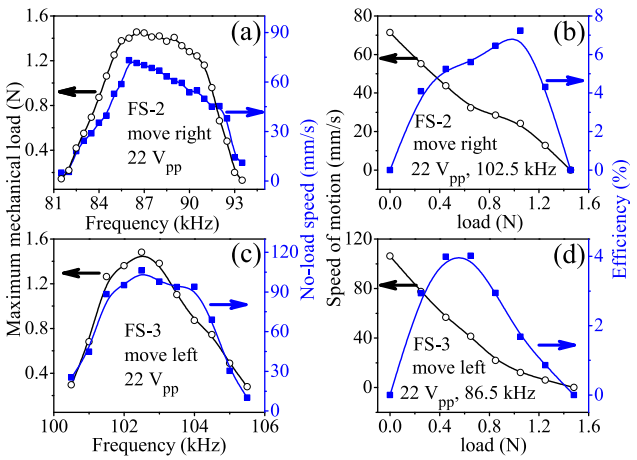

FIG. 5. Performances of the USM, (a) and (c) the maximum mechanical load and no-load speed as a function of working frequency, (b) and (d) speed of motion and efficiency as a function of mechanical load.

by mode splitting—a prevalent problem in conventional L1-B2 piezoelectric linear motors when subjected to a temperature change.[23,28]

In summary, we investigated the asymmetric and non-isomorphic high-order face-shear vibration modes of [011] poled Zt ± 45° cut relaxor-PT crystals and their application for the USM. The crystal exhibited asymmetric face-shear mode deformations, and unlike the piezoelectric ceramic, its two high-order face-shear modes degraded to two non-isomorphic modes. A standing wave linear USM was presented which exhibited a relatively large driving force (1.5 N) in bi-directional motion under a relatively low driving voltage (22 V_{pp}). These findings could provide guidance for design of resonance devices based on relaxor-PT crystals operating in high-order face-shear vibration modes.

This work was sponsored by the National Natural Science Foundation of China (Grant Nos. 50872002, 51132001, and 11090331). Authors acknowledge the collaborations of Heidstar Company, Xiamen, China.

[1]J. Chen and R. Panda, in *IEEE Ultrasonics Symposium* (IEEE, Piscataway, NJ, 2005), pp. 235–240.
[2]H. C. Robinson, "Single crystal projectors for compact, broadband sonar," in Proceedings of the 2011 IEEE International Symposium on Applied Ferroelectrics, Vancouver, Canada, 24–27 July 2011.
[3]C. H. Sherman and J. L. Butler, *Transducers and Arrays for Underwater Sound* (Springer, NY, 2007).
[4]Z. Li, A. Huang, G. Luan, and J. Zhang, Ultrasonics **44**(Supplement), e759 (2006).
[5]D. R. Patil, R. C. Kambale, Y. Chai, W.-H. Yoon, D.-Y. Jeong, D.-S. Park, J.-W. Kim, J.-J. Choi, C.-W. Ahn, B.-D. Hahn *et al.*, Appl. Phys. Lett. **103**(5), 052907 (2013).
[6]K. A. Cook-Chennault, N. Thambi, and A. M. Sastry, Smart. Mater. Struct. **17**(4), 043001 (2008).
[7]Z. Hu, B. Ma, S. Liu, M. Narayanan, and U. Balachandran, Ceram. Int. **40**(1), 557 (2014).
[8]X. Jiang, W. B. Cook, and W. S. Hackenberger, Proc. SPIE **7439**, 74390Z (2009).
[9]S. Zhang and F. Li, J. Appl. Phys. **111**(3), 031301 (2012).
[10]C. L. Zhang, W. Chen, and J. Yang, Int. J. Appl. Electromagn. Mech. **31**(4), 207 (2009).
[11]Q. Zhou, X. Xu, E. J. Gottlieb, L. Sun, J. M. Cannata, H. Ameri, M. S. Humayun, P. Han, and K. K. Shung, IEEE Trans. Ultrason. Ferroelectr. Freq. Control **54**(3), 668 (2007).
[12]S. Zhang, F. Li, W. Jiang, J. Luo, J. Richard, J. Meyer, W. Cao, and T. R. Shrout, Appl. Phys. Lett. **98**(18), 182903 (2011).
[13]S. Zhang, W. Jiang, J. Richard, J. Meyer, F. Li, J. Luo, and W. Cao, J. Appl. Phys. **110**(6), 064106 (2011).
[14]S. Li, W. Jiang, L. Zheng, and W. Cao, Appl. Phys. Lett. **102**(18), 183512 (2013).
[15]C. Zhan, J. Wu, S. Yin, and X. Jiang, J. Appl. Phys. **97**(7), 074107 (2005).
[16]S. Priya, J. Ryu, K. Uchino, and D. Viehland, Appl. Phys. Lett. **79**(16), 2624 (2001).
[17]X.-H. Du, Q.-M. Wang, and K. Uchino, IEEE Trans. Ultrason. Ferroelectr. Freq. Control **51**(2), 238 (2004).
[18]F. Li, S. Zhang, Z. Xu, X. Wei, J. Luo, and T. R. Shrout, Appl. Phys. Lett. **96**(19), 192903 (2010).
[19]Z. Li, Z. Xu, Z. Xi, L. Cao, and X. Yao, J. Electroceram. **21**(1–4), 279 (2008).
[20]F. Martin, H. ter Brake, L. Lebrun, S. Zhang, and T. Shrout, J. Appl. Phys. **111**(10), 104108 (2012).
[21]K. Uchino, *Ferroelectric Devices* (CRC, 2000).
[22]P. Ci, Z. Chen, G. Liu, and S. Dong, IEEE Trans. Ultrason. Ferroelectr. Freq. Control **61**(1), 159 (2014).
[23]P. Ci, G. Liu, Z. Chen, and S. Dong, Appl. Phys. Lett. **103**(10), 102904 (2013).
[24]K. Kim, S. Zhang, and X. Jiang, Appl. Phys. Lett. **100**(25), 253501 (2012).
[25]K. Kim, S. Zhang, and X. Jiang, IEEE Trans. Ultrason. Ferroelectr. Freq. Control **59**(11), 2548 (2012).
[26]W. Y. Chang, W. B. Huang, A. Bagal, C. H. Chang, J. Tian, P. D. Han, and X. N. Jiang, J. Appl. Phys. **114**(11), 114103 (2013).
[27]Z. J. Chen, X. T. Li, J. G. Chen, and S. X. Dong, IEEE Trans. Ultrason. Ferroelectr. Freq. Control **60**(1), 115 (2013).
[28]X. Li, J. Chen, Z. Chen, and S. Dong, Appl. Phys. Lett. **101**(7), 072902 (2012).